



UNIVERSITY OF LEEDS

This is a repository copy of *Solvent-assisted synthesis of potassium copper hexacyanoferrate embedded 3D-interconnected porous hydrogel for highly selective and rapid cesium ion removal.*

White Rose Research Online URL for this paper:  
<http://eprints.whiterose.ac.uk/111376/>

Version: Accepted Version

---

**Article:**

Kim, YK, Kim, Y, Kim, S et al. (2 more authors) (2017) Solvent-assisted synthesis of potassium copper hexacyanoferrate embedded 3D-interconnected porous hydrogel for highly selective and rapid cesium ion removal. *Journal of Environmental Chemical Engineering*, 5 (1). pp. 975-986. ISSN 2213-3437

<https://doi.org/10.1016/j.jece.2017.01.026>

---

© 2017 Elsevier Ltd. This manuscript version is made available under the CC-BY-NC-ND 4.0 license <http://creativecommons.org/licenses/by-nc-nd/4.0/>

**Reuse**

Unless indicated otherwise, fulltext items are protected by copyright with all rights reserved. The copyright exception in section 29 of the Copyright, Designs and Patents Act 1988 allows the making of a single copy solely for the purpose of non-commercial research or private study within the limits of fair dealing. The publisher or other rights-holder may allow further reproduction and re-use of this version - refer to the White Rose Research Online record for this item. Where records identify the publisher as the copyright holder, users can verify any specific terms of use on the publisher's website.

**Takedown**

If you consider content in White Rose Research Online to be in breach of UK law, please notify us by emailing [eprints@whiterose.ac.uk](mailto:eprints@whiterose.ac.uk) including the URL of the record and the reason for the withdrawal request.

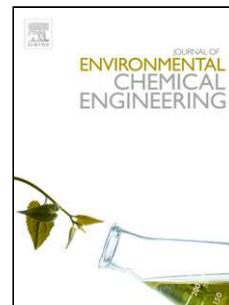


[eprints@whiterose.ac.uk](mailto:eprints@whiterose.ac.uk)  
<https://eprints.whiterose.ac.uk/>

## Accepted Manuscript

Title: Solvent-assisted Synthesis of Potassium Copper Hexacyanoferrate embedded 3D-Interconnected Porous Hydrogel for Highly Selective and Rapid Cesium Ion Removal

Authors: Yun Kon Kim, Yonghwan Kim, Sungjun Kim, David Harbottle, Jae W. Lee



PII: S2213-3437(17)30026-X  
DOI: <http://dx.doi.org/doi:10.1016/j.jece.2017.01.026>  
Reference: JECE 1441

To appear in:

Received date: 10-11-2016  
Revised date: 22-12-2016  
Accepted date: 19-1-2017

Please cite this article as: Yun Kon Kim, Yonghwan Kim, Sungjun Kim, David Harbottle, Jae W.Lee, Solvent-assisted Synthesis of Potassium Copper Hexacyanoferrate embedded 3D-Interconnected Porous Hydrogel for Highly Selective and Rapid Cesium Ion Removal, Journal of Environmental Chemical Engineering <http://dx.doi.org/10.1016/j.jece.2017.01.026>

This is a PDF file of an unedited manuscript that has been accepted for publication. As a service to our customers we are providing this early version of the manuscript. The manuscript will undergo copyediting, typesetting, and review of the resulting proof before it is published in its final form. Please note that during the production process errors may be discovered which could affect the content, and all legal disclaimers that apply to the journal pertain.

**Solvent-assisted Synthesis of Potassium Copper Hexacyanoferrate embedded 3D-  
Interconnected Porous Hydrogel for Highly Selective and Rapid Cesium Ion Removal**

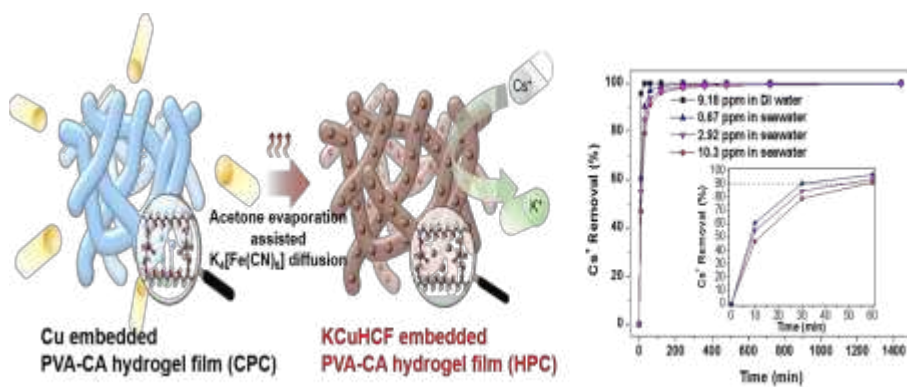
Yun Kon Kim<sup>a</sup>, Yonghwan Kim<sup>a</sup>, Sungjun Kim<sup>a</sup>, David Harbottle<sup>b</sup> and Jae W. Lee<sup>a\*</sup>

<sup>a</sup>Department of Chemical and Biomolecular Engineering, Korea Advanced Institute of  
Science and Technology (KAIST), Daejeon 305-701, Republic of Korea

<sup>b</sup>School of Chemical and Process Engineering, University of Leeds, Leeds LS2 9JT, United  
Kingdom

KEYWORDS: Cesium removal, Fukushima, Potassium copper hexacyanoferrate,

Poly(vinyl alcohol) hydrogel.



The KCuHCF embedded PVA-Citric acid hydrogel adsorbent was synthesized through a facile two-step method for the selective and rapid  $Cs^+$  removal.

## Highlights

- The HPC was synthesized by a noble solvent-assisted method.
- The HPC showed superior Cs<sup>+</sup> removal capacity of 667 mg/g KCuHCF.
- The HPC retained remarkable Cs<sup>+</sup> removal efficiency of 99.5 % in 30 min.
- In a wide pH range from 2 to 10, the HPC displayed stable Cs<sup>+</sup> removal efficiency.

**Abstract**

Potassium copper hexacyanoferrate-embedded poly(vinyl alcohol)-citric acid hydrogel film (HPC) was prepared via a two-step method of Cu immobilization, followed by the diffusion of potassium hexacyanoferrate accelerated by acetone evaporation. The diffusion-derived KCuHCF formation in the preformed hydrogel facilitated the preservation of the 3D-interconnected hydrogel structure and dispersion of the KCuHCF nanoparticles. Using acetone as a non-solvent, reverse diffusion of the incorporated Cu in the hydrogel matrix was hindered; hence a large amount of KCuHCF was loaded in the matrix. The HPC exhibited substantially enhanced  $\text{Cs}^+$  removal properties in terms of adsorption capacity, kinetics and selectivity. From the adsorption isotherm, the HPC showed a very high  $\text{Cs}^+$  uptake of 667 mg/g KCuHCF. Moreover, the adsorbent revealed stable and high  $\text{Cs}^+$  removal efficiency of 99.9 % across a wide pH range from 2 to 10. The kinetics of  $\text{Cs}^+$  removal was remarkably rapid with 99.5% removal achieved within 30 min from a dilute  $\text{Cs}^+$  solution (9.18 ppm). When using seawater, the HPC exhibited almost unaltered  $\text{Cs}^+$  removal efficiency above 99.5 %, and high distribution coefficient  $K_d$  value of  $7.7 \times 10^5$  mL/g at an extremely low  $\text{Cs}^+$  concentration (0.67 ppm,  $V/m = 1000$  ml/g), which highlighted the tremendous affinity for  $\text{Cs}^+$ .

## 1. Introduction

To meet our energy needs in the 21st century, nuclear power has emerged as one of the most promising alternatives to fossil fuels, providing approximately 9.7 % of the world's energy [1]. However, from an environmental perspective, nuclear energy can pose a threat due to the release of approximately 2000-2300 metric tons of radioactive waste into the environment each year [1]. Thus, for the continuous and long-term operation of nuclear facilities, environmental remediation and confinement of generated wastes remain a key priority [2]. Aside from the issues of operational radioactive effluent, nuclear incidents such as those witnessed at Fukushima Daiichi, and Chernobyl have resulted in the long-term and catastrophic contamination of the biosphere, hence issues around accident tolerant power plants are also being addressed [3].

Among all the radioactive elements, gamma ray emitters  $^{134}\text{Cs}$  and  $^{137}\text{Cs}$  are the richest and the most hazardous nuclear fission products of uranium [4-6]. Both isotopes are considerably harmful to humans and can easily destroy the environmental habitat since they can quickly migrate through ground and sea waters, accumulating in the biosphere for hundreds of years [5].

Ion exchange with an inorganic adsorbent is a promising technology for the recovery of radioactive elements from nuclear waste streams due to its convenience (availability), effectiveness and high adsorptive capacity. Zeolites [7, 8], crystalline silicotitanates [9, 10], chalcogenides [11-13], and clay minerals [14, 15], are common inorganic ion exchangers, however, their low selectivity for Cs over other competitive

elements such as Na, K, Mg, Co, Ni or actinides, inhibits their practical application for large scale processes [5].

In the last few decades, the transition metal based hexacyanoferrate (HCF) has demonstrated excellent ion exchange properties for the selective separation of  $\text{Cs}^+$ , even in a large excess of co-existing competing cations ( $\text{Na}^+$ ,  $\text{K}^+$ ,  $\text{Mg}^{2+}$ ,  $\text{Ca}^{2+}$ , ...), which are often present in contaminated effluents [1, 4, 5, 16-18]. Since metal HCF has a well-known perovskite-like face-centered cubic crystal structure, with a channel diameter of around 3.2 Å, small hydrated cations such as  $\text{Cs}^+$  can be inserted, whereas the larger hydrated ions such as  $\text{Na}^+$  are selectively rejected [4, 19]. Particularly, copper hexacyanoferrate has been widely used due to its simple preparation, low cost, superior  $\text{Cs}^+$  capture properties, and chemical stability over a wide pH range [3, 17, 18, 20]. In spite of the advantageous structural properties for the selective removal of  $\text{Cs}^+$ , one of the main drawbacks of the adsorbent is related to its ultra-fine particle size, increasing the difficulty to remove the occupied ion exchangers following adsorption [21]. Furthermore, the nano-sized particles hinder their direct application for fixed-bed column operations due to the high pressure drop and channel blocking.

In order to address such issues, numerous studies have considered the immobilization of the small sized metal HCF particles, either by grafting onto porous media [5, 16, 20, 22], or encapsulating in a polymer matrix [1, 3, 23, 24]. Turgis et al. reported a method using copper-catalyzed azide-alkyne cycloaddition (CuAAC) “click reaction” to retain CuHCF on functionalized mesoporous silica [16]. Vincent et al. showed a facile synthesis method by encapsulating metal (Cu, Ni, Co, Zn or Fe) HCF

with chitin beads [3]. Although these studies demonstrated promising technologies for the incorporation of metal HCF, the performance remained somewhat limited due to low adsorption capacity, slow kinetics, accessibility, and reduced availability of reactive groups. In the case of impregnation in porous materials, only a small quantity of HCF was dispersed in the support, thus  $\text{Cs}^+$  adsorption capacity of the composite was very low. The application of encapsulation using polymers such as chitosan, or alginate leads to the aggregation of the HCF particles in the polymer matrix, which decreases the accessibility of  $\text{Cs}^+$  to ion-exchange sites and reduces sorption properties.

To overcome these performance barriers, this study proposes a sequential two-step synthesis of potassium copper hexacyanoferrate (KCuHCF) nanoparticles embedded in a crosslinked polymer hydrogel film (Fig. 1(a)). Immobilization of Cu in the polymer hydrogel matrix was performed, followed by the acetone-assisted evaporative diffusion of  $\text{K}_4[\text{Fe}(\text{CN})_6]$  into the preformed film structure to induce the formation of KCuHCF in the matrix. Therefore, the hydrogel film structure was entirely maintained and KCuHCF nanoparticles were well dispersed in the 3D-interconnected network. Furthermore, in the diffusion step, acetone is introduced to restrict the disintegration of incorporated Cu, so the high loading of KCuHCF in the film was realized. For this purpose, poly(vinyl alcohol) (PVA) and citric acid were utilized as the polymer backbone and crosslinking agent due to their low cost, nontoxicity, and hydrophilic properties [25, 26]. In addition, the components have abundant oxygen functionalities such as hydroxyl or carboxyl groups which can coordinate metal ions for anchoring and distribution of KCuHCF particles [23, 26].

Together with the physicochemical properties of the synthesized KCuHCF-embedded PVA-citric acid hydrogel (HPC), the adsorption performance was evaluated with respect to the equilibrium capacity, removal efficiency, kinetics, selectivity, and stability. The research showed significant  $\text{Cs}^+$  uptake normalized by the weight of loaded KCuHCF. Distinctly, the HPC exhibited very fast  $\text{Cs}^+$  removal kinetics and superior removal efficiency above 99.5% in seawater, even with a very low concentration of  $\text{Cs}^+$ . These remarkable adsorption characteristics demonstrate HPC to be a very attractive and promising candidate for the separation of  $\text{Cs}^+$  from nuclear waste effluents.

## 2. Materials and methods

### 2.1. Materials

Poly (vinyl alcohol) (PVA,  $M_w$  89,000–98,000 g/mol, 99+% hydrolyzed), citric acid ( $\geq 99.5$  %), potassium hexacyanoferrate (II) trihydrate ( $\text{K}_4[\text{Fe}(\text{CN})_6] \cdot 3\text{H}_2\text{O}$ ,  $\geq 99.5$  %), and untreated seawater were acquired from Sigma-Aldrich and used as received. Copper sulfate pentahydrate ( $\text{CuSO}_4 \cdot 5\text{H}_2\text{O}$ , KANTO Chemical Co. Inc.) and cesium chloride ( $\text{CsCl}$ , 99.9 %, Alfa Aesar) were also used as received. Hydrochloric acid ( $\text{HCl}$ ) was purchased from the OCI Company. Sodium hydroxide and acetic acid were commercially available from JUNSEI. Milli-Q deionized (DI) water ( $18.2 \text{ M}\Omega \text{ cm}^{-1}$ ) and acetone were used for the synthesis and solution preparation.

## 2.2. Synthesis of the KCuHCF embedded PVA-citric acid hydrogel film (HPC)

The HPC was synthesized using a two-step procedure (Fig. 1(b)). In the first step, the Cu embedded film (Cu embedded PVA-citric acid: CPC) was formed. Typically, 0.5 g of PVA was dissolved into DI water (5 wt% PVA solution) at 90 °C for 1 h with vigorous stirring. The mixture solution (15 ml) of citric acid and CuSO<sub>4</sub> was added to the prepared PVA solution under vigorous stirring for 2 h at 30 °C, with the mass ratio between PVA and citric acid set to 1:0.6, and the molar ratio of citric acid to CuSO<sub>4</sub> was equal to 2. Then the homogeneous solution was cast onto a teflon dish, and heated from 60 to 120 °C at a heating rate of 1 °C/min and maintained for 2 h in an oven, where crosslinking between PVA and citric acid occurred and the CPC was formed. In the second step, the CPC was added to a 100 ml of 1 M K<sub>4</sub>[Fe(CN)<sub>6</sub>] aqueous solution and then stirred for 24 h. The reaction conditions were additionally controlled as given in Table 1, depending on the addition of 200 ml acetone to the aqueous solution with or without the heat-treatment at 35 °C for the first 2 hours. The formed HPC was washed with DI water and acetone, followed by drying the HPC in an oven at 30 °C for 24 h.

The PVA-citric acid hydrogel film (PC) was prepared as a reference sample following the same procedure previously described, except for the addition of CuSO<sub>4</sub>. The synthesized PC was stored under vacuum for further physicochemical characterization and adsorption studies.

### 2.3. Synthesis of bulk KCuHCF

The bulk KCuHCF nanoparticles have been prepared via the reaction of soluble potassium hexacyanoferrate and metal salt. In this study, KCuHCF nanoparticles were synthesized by adding  $K_4[Fe(CN)_6]$  (50 ml, 0.05 M) dropwise into  $CuSO_4$  solution (50 ml, 0.06 M) until reddish-brown precipitates were formed. The colloidal solution was continuously stirred for 4 h at room temperature. The synthesized KCuHCF nanoparticles were washed several times with DI water to remove residual salts and impurities, and isolated by centrifugation. Finally, the nanoparticles were dried in an oven at 90 °C for 24 h.

### 2.4. Characterizations

The morphology of the prepared sample was observed by scanning electron microscopy (SEM, Magellan 400 UHR-SEM at 1kV, FEI Company, USA), combined with an energy dispersive analysis of X-rays (EDS, OCTANE SUPER 60mm<sup>2</sup>, EDAX, USA). To observe the swelled open-pore structure, the PC and HPC samples were immersed in DI water and freeze-dried at -53 °C. Transmission electron micrographs (TEM) were taken on a JEOL JEM-2100F at 200 kV (JEOL, Ltd, Japan). Before the TEM analysis, the HPC was size reduced by grinding and dissolved in 1 wt% acetic acid aqueous solution with uninterrupted stirring at 85 °C, followed by the dropwise addition of the solution onto a nickel-grid. The nitrogen adsorption and desorption isotherm was obtained at 77 K with Micromeritics (USA) 3Flex after degassing the sample under high vacuum at 75 °C. Film and powder x-ray diffraction (XRD) were carried out on a RIGAKU (Japan) D/MAX-2500 (Cu  $K\alpha$ ,  $\lambda = 1.54059 \text{ \AA}$ , 40 kV and

300 mA) and Smartlab (Cu K $\alpha$ ,  $\lambda = 1.54059 \text{ \AA}$ , 45 kV and 200 mA), respectively. X-ray photoelectron spectroscopy (XPS) was conducted on a K-alpha (Thermo Fisher Scientific, USA) and Fourier transform infrared spectra (FTIR) were measured with an attenuated total reflectance (ATR) crystal of a Nicolet iS50 (Thermo Fisher Scientific, USA) from 400 to 4000  $\text{cm}^{-1}$ , to identify the chemical bonding and composition of the as-prepared adsorbents. The metal composition of the adsorbent was precisely determined by inductively coupled plasma optical emission spectroscopy (ICP-OES 720, Agilent, USA) after dissolution of the sample in a mixture of  $\text{HNO}_3$  and  $\text{HCl}$  at an elevated temperature.

## 2.5. $\text{Cs}^+$ Adsorption Experiments

All adsorption studies were performed using 1000 ml/g basis of solution to dried adsorbent mass (V/m). Initial and specific  $\text{Cs}^+$  concentrations in the aqueous phase were quantified in triplicate using an inductively coupled plasma mass spectrometer (ICP-MS 7700S, Agilent, USA) and the average concentration was reported.

The ion exchange experiment was performed with the prepared HPC and bulk KCuHCF in an excess amount of 0.01 M  $\text{Cs}^+$  solution, in which V/m was equal to 1000 ml/g. The mixture was shaken for 24 h at 25 °C. The ion exchange materials were washed several times with DI water and acetone, and paper-filtered or isolated by centrifugation, before oven drying the ion exchanged HPC and bulk KCuHCF.

For the determination of adsorption isotherms, 20 mg of adsorbent was shaken in 20 ml Cs<sup>+</sup> solution at 25 °C by varying the initial Cs<sup>+</sup> concentration (C<sub>0</sub>). After 24 h of contact, the adsorbent was separated from the liquid phase using 0.45 µm Whatman syringe filter and the residual Cs<sup>+</sup> concentration (C<sub>e</sub>) in the filtrate was measured by ICP-MS. The adsorption capacity was calculated by equation (1)

$$q_e = (C_0 - C_e) \times V/m \quad (1)$$

where C<sub>0</sub> and C<sub>e</sub> are the initial and equilibrium concentrations of Cs<sup>+</sup> (mg/L) in the aqueous phase, respectively. V is the volume of the solution (L), m is the weight of adsorbent (g), and q<sub>e</sub> is the adsorption amount of adsorbate per unit weight of adsorbent (mg/g).

The kinetic adsorption of cesium from both DI water and seawater was completed by shaking the sample adsorbent in 0.6 to 10 ppm of Cs<sup>+</sup> solution at 25 °C, and 1 mL aliquots were sampled at regular intervals between 10 min and 24 h for ICP-MS analysis. For each experiment, 200 mg of adsorbent was dispersed in 200 ml of Cs<sup>+</sup> containing solution. The removal efficiency (RE) was determined from the difference between the initial concentration (C<sub>0</sub>) and the concentration (C<sub>t</sub>) at each sampling time interval:

$$RE = (C_0 - C_t)/C_0 \times 100 \quad (\%) \quad (2)$$

The distribution coefficient (K<sub>d</sub>, ml/g) was applied to determine the Cs<sup>+</sup> affinity of the HPC and the bulk KCuHCF over competing cations:

$$K_d = \frac{(C_0 - C_e)}{C_e} \left( \frac{V}{m} \right) \quad (3)$$

where  $C_0$  and  $C_e$  are the initial and equilibrium concentration of  $Cs^+$  (mg/L) in the aqueous phase, respectively.  $V$  is the solution volume (mL) and  $m$  is the weight of adsorbents (g).

The pH-dependent  $Cs^+$  removal efficiency was also evaluated by immersing 50 mg of the HPC in 50 ml  $Cs^+$  solution at 25 °C with a contact time of 24 h. The pH of the 11ppm  $Cs^+$  solution ( $C_0 \approx 11$  ppm) was adjusted using HCl or NaOH, with the pH confirmed by a digital pH meter (Mettler Toledo S220, Swiss).

## 2.6. Swelling measurements

The swelling kinetics of HPC was performed by immersing the dried HPC in both DI water and seawater at 25 °C. At specified time intervals, the hydrogel was recovered from the aqueous environment and any excess water on the surface of the hydrogel was removed by filter paper before weighing. The swelling ratio (SR) was calculated as follows

$$SR = (W_s - W_d)/W_d \quad (4)$$

where  $W_s$  is the swelled weight of the hydrogel (g) at time  $t$ , and  $W_d$  is the weight of the dried hydrogel (g).

### 3. Results and Discussion

#### 3.1 Solvent-assisted KCuHCF dispersion in the HPC synthesis

The HPC adsorbent embedded with highly dispersed KCuHCF nanoparticles was prepared via a two-step method (Fig. 1(b)). The first step was used to immobilize and distribute Cu in the CPC film structure using the abundant oxygen functional groups in PVA and citric acid [23]. Next, both acetone-treatment and heat-treatment were used according to the conditions presented in Table 1. Acetone was used as a non-solvent to restrict the reverse diffusion of deposited Cu from the CPC polymer matrix, and heat-treatment was applied to drive the fast diffusion of  $K_4[Fe(CN)_6]$  into the CPC structure.

To determine the effect of both acetone- and heat-treatments, four experiments were designed using the four different conditions as outlined in Table 1. The weight fractions of Cu and Fe are displayed in the prepared adsorbents. Initially, the pristine CPC immobilized 5.23 wt% Cu based on the weight of PVA and citric acid. In each DI water condition (W group: W-RT and W-35), the retained Cu content significantly decreased to 2.15 and 2.77 wt%, while the addition of the acetone (WA group: WA-RT and WA-35) resulted in a greater retention of Cu (4.02 and 4.18 wt%), by suppressing the reverse diffusion back to the solution phase.

The differences in Fe composition for each sample in W (1.37 wt% of W-RT vs 1.77 wt% of W-35) and WA (1.16 wt% of WA-RT vs 3.41 wt% of WA-35), indicate that the heat-treatment increased the diffusion rate of  $K_4[Fe(CN)_6]$  into the

CPC. Although heating increases the diffusion rate of both  $K_4[Fe(CN)_6]$  and Cu, the confinement of Cu by the matrix makes the reverse diffusion rate of Cu lower. Moreover, the higher content of Cu in W-35 and WA-35 than in W-RT and WA-RT is positively related to the rapid mass transfer of  $K_4[Fe(CN)_6]$  at the higher temperature, because KCuHCF is formed by the reaction between Cu and  $K_4[Fe(CN)_6]$  in the film structure and becomes immobilized in the matrix.

Unlike WA-RT, acetone in WA-35 was evaporated during the heat-treatment, gradually inducing the water-rich solution phase leading to an increase in the  $K_4[Fe(CN)_6]$  solubility (refer to Fig. S1 in the Supplementary Material). These results suggest that the combined acetone-treatment and heat-treatment were required to achieve the high retention of KCuHCF in the film structure. Therefore, all HPC samples used for performance testing were formed via the WA-35 method.

### 3.2. Characterization: physical properties

The internal 3D structure of the hydrogel film was investigated by SEM. Fig. 2 compares the porous macrostructure of the as-synthesized PC and HPC (refer to more images provided in Fig. S2). Both films have an interconnected porous structure with different pore size distributions and wall structures. The PC, as illustrated in Fig. 2(a), shows a highly distributed porous structure with pore sizes ranging from 0.6 to 1.5  $\mu\text{m}$ . However, the HPC (Fig. 2(b)) exhibits larger pores in the range of 1 - 2.5  $\mu\text{m}$  and a thicker wall structure, because Cu incorporation decreases the participation of citric acid as a crosslinking agent [27-29].

At higher magnification, Fig. 2(c) exhibits an uneven film surface, revealing the confinement of KCuHCF in the film. The compositional homogeneity of the dispersed nanoparticles was identified by EDS analysis (Fig. 2(d)) using single point measurements along a cross section of the porous film surface (as shown by the gray line in Fig. 2(b)). The measured atomic ratios of Fe and Cu are almost constant (average Fe/Cu = 0.59) with an average deviation less than 10 %, thus demonstrating that the chemical composition of the immobilized KCuHCF remains uniform throughout. Furthermore, the elemental mapping analysis of the HPC clearly supports the dispersion of the KCuHCF throughout the hydrogel structure (Fig. S3).

The bulk KCuHCF nanoparticles appear cubic structure (Fig. S4), and the TEM image (Fig. 2(e)) indicates aggregation of the nano-crystallites with an average size between 9-15 nm. In contrast, the KCuHCF nanoparticles (Fig. 2(f)) in the HPC are well dispersed across the whole film framework, with very few shape irregularities which can be attributed to few aggregations of the smaller particles [30]. Although most of the ground PVA specimens are solubilized in 1 wt% acetic acid solution, the presence of a residual layer of the matrix inhibits aggregation of the nanoparticles [31, 32]. At higher magnification (Fig. 2(f) inset), the measured size of nanoparticles was approximately 12 nm, which corresponds to the mean size of  $12.3 \pm 5.7$  nm determined from the Gaussian particle size distribution (Fig. S5).

The mesoporous property of the HPC was determined from the nitrogen sorption isotherm, BJH and NLDFIT pore size distributions (PSDs). The isotherm (Fig. 3) represents a type IV shape according to the IUPAC classification with hysteresis

loop at  $P/P_0 = 0.8\sim 1$ , implying the mesoporous structure, and the BET surface area and the total pore volume at  $P/P_0 = 0.996$  are  $53 \text{ m}^2/\text{g}$  and  $0.47 \text{ cm}^3/\text{g}$ , respectively. The BJH PSD (Fig. S6) calculated from the desorption branch shows a wide distribution between 10-50 nm. Moreover, the NLDFT model (Fig. 3 inset) also indicates a broad mesopore distribution and a steep increase of cumulative volume from 10 to 60 nm. Therefore, the  $\text{N}_2$  adsorption isotherm clearly demonstrates the broad range of mesoporosity in the HPC along with macropores as revealed in the SEM analyses.

### 3.3. Characterization: chemical properties

The XRD patterns of the prepared films and the bulk KCuHCF are shown in Fig. 4(a). Both PC and CPC show a PVA related main peak centered at  $19.4^\circ$  [33]. For CPC, no Cu related peaks are observed in the diffraction pattern, meaning that the incorporated Cu particles are not in the form of single crystallites [34]. Though the low intensity peak at around  $30^\circ$  is hardly recognizable in the HPC, the peaks of the HPC and bulk KCuHCF (Fig. 4(a)) are similar, except for an intense reflection from the film matrix at  $19.4^\circ$ . From the specific peak patterns, it can be concluded that they have very similar crystalline structures.  $2\theta$  values around  $18^\circ$ ,  $25^\circ$ ,  $36^\circ$ ,  $40^\circ$ ,  $44^\circ$ ,  $52^\circ$ ,  $55^\circ$ , and  $58^\circ$  are assigned to Miller indexes of (200), (220), (400), (420), (422), (440), (600), and (620) reflections, respectively, which corresponds to the intrinsic peaks of  $\text{K}_2\text{Cu}[\text{Fe}(\text{CN})_6]$  (PDF no. 01-075-0023) [3, 6, 16, 35]. The average particle size of KCuHCF is determined to be  $\sim 9$  and  $\sim 12$  nm for the HPC and the bulk form, respectively, using Scherrer equation at diffraction points of  $18^\circ$  and  $36^\circ$  [35]. In both cases, the calculated values are slightly smaller than the observed particle size in the

TEM analysis (Fig. 2(e) and 2(f)), because of little aggregation of the smaller nanoparticles [36].

The characteristics of the chemical bonding and transformation were investigated by FTIR measurements. The IR spectra of the bulk KCuHCF and the synthesized films are shown in Fig. 4(b). The prepared bulk KCuHCF exhibits a sharp peak at  $2072\text{ cm}^{-1}$  indicative of the characteristic stretching vibration of  $\text{C}\equiv\text{N}$ , and less intense bands around  $590$  and  $475\text{ cm}^{-1}$ , which are assigned to Fe-CN deformation and Cu-CN stretching mode, respectively [3, 6, 18, 37]. The low intense peak at  $1606\text{ cm}^{-1}$  is attributed to lattice water [37]. In the case of the PC and HPC, the strong absorbance at around  $1719$  and  $1208\text{ cm}^{-1}$  indicates the stretching vibrations of  $\text{C}=\text{O}$  and  $\text{C}-\text{O}-\text{C}$  relating to the esterification reaction between  $-\text{OH}$  in poly(vinyl alcohol) and  $-\text{COOH}$  in citric acid [26, 38]. A broad and strong band covering the range  $3000\text{-}3700\text{ cm}^{-1}$  relates to the symmetrical stretching vibration from inter and intramolecular hydrogen bonds of O-H [39]. The peak at around  $2922\text{ cm}^{-1}$  is attributed to C-H stretching from  $-\text{CH}_2-$  [40]. For the HPC, the peak appearance at  $1597$  and  $1416\text{ cm}^{-1}$  is due to  $\text{COO}^-$  antisymmetric and symmetric stretching, respectively, suggesting the binding of potassium with  $\text{COO}^-$  [41, 42]. The functional group of  $\text{COO}^- \text{K}^+$  could be originated from the carboxylate of citric acid coordinated to Cu after the formation of KCuHCF, and the presence of Cu-CA complex in the CPC is confirmed by the shoulder peak at  $1621\text{ cm}^{-1}$  [43]. In addition, the distinct bands at  $2089$ ,  $586$ , and  $478\text{ cm}^{-1}$  in the HPC clearly demonstrate the existence of KCuHCF, where the shift of  $\text{C}\equiv\text{N}$  stretching compared to that of the bulk KCuHCF is related to the internal strain in the film matrix [44].

X-ray photoelectron spectroscopy (XPS) was completed on the samples to determine the chemical bonding and valence states of Fe on the prepared adsorbent surface. The C1s core level spectra of the HPC are shown in Fig. 5(a). The carbon bondings are classified into the four different peaks centered at 284.5, 285.9, 287.3 and 288.8 eV corresponding to C-C, C-O in the polymer backbone, C≡N in the KCuHCF and O-C=O in ester and carboxylate, respectively [45]. Thus, along with the IR spectra, XPS results confirm the successful crosslinking reaction, and the presence of carboxylate and dispersion of the KCuHCF in the HPC. Fig. 5(b) displays the Fe2p core level spectra of both HPC and bulk KCuHCF. Since the KCuHCF nanoparticles are embedded in the interior of the film, the measured spectra for the HPC show a lower intensity and resolution than the bulk KCuHCF. However, the two peaks in the respective spectra are sufficiently distinguished (708.4, 720.9 eV for the HPC and 708.6, 721.3 eV for the bulk) revealing that both adsorbents have the identical Fe<sup>2+</sup> valence state [46].

Considering the XRD patterns ( $K_2Cu[Fe(CN)_6]$ ) and XPS results, the stoichiometric ratio of the nanoparticles is set as  $K_{4x-2}Cu[Fe(CN)_6]_x$  from the ICP-OES results in Table 2. The calculated chemical composition for the HPC and bulk is noticeably different. In the case of the HPC, Cu to Fe ratio is close to 1 (i.e. the reaction of one Cu per one  $Fe(CN)_6$ ), but for the bulk species, Cu content is much higher than Fe by approximately 1.5 times (i.e. reaction of 1.5 Cu per one  $Fe(CN)_6$ ). Concerning the preparation step, Cu is dispersed and immobilized in the film matrix by the oxygen functional groups of PVA and citric acid, thus the limiting reactant (Cu)

reacts with the surrounding excess of  $\text{Fe}(\text{CN})_6$  via a one-to-one stoichiometry and the negative charge is compensated by potassium ions.

Assuming that  $\text{Cs}^+$  adsorption is mainly accompanied by the ion exchange with  $\text{K}^+$  as reported in previous studies [3, 35, 47], the theoretical ion exchange capacity (TEC) is calculated from the amount of  $\text{K}^+$  in  $\text{KCuHCF}$  (Table 2). The HPC shows much higher theoretical adsorption capacity than the bulk  $\text{KCuHCF}$ , which will be discussed later with the adsorption isotherm study. The ion exchanger content (IEC) in the HPC was determined to be 17.46 wt% depending on the stoichiometry and measured weight fraction of K, Cu and Fe. Besides the amounts of potassium determined by stoichiometry, the ICP-OES results for the HPC also confirm the excess amount of  $\text{K}^+$ , demonstrating the bonding with carboxylate in citric acid as proved in the FTIR spectra (Fig. 4(b)).

### 3.4. Ion exchange of $\text{KCuHCF}$ with $\text{Cs}^+$

To investigate the ion exchange mechanism of  $\text{KCuHCF}$ , XPS, FTIR, and XRD measurements were completed on the HPC (Fig. 6) and the bulk (Fig. S7) samples following adsorption in high  $\text{Cs}^+$  concentration (0.01 M) for 24 h. In the XPS spectra, the peaks for  $\text{K}^+$  (Fig. 6(a)) are not identified compared to  $\text{K}2\text{p}$  spectra for the pristine HPC (Fig. 6(a) inset). However, the characteristic  $3\text{d}_{5/2}$  and  $3\text{d}_{3/2}$  for  $\text{Cs}^+$  (Fig. 6(b)) at 724.2 and 738.1 eV are clearly observed following adsorption. The FTIR analysis (Fig. 6(c)) shows a shift of the  $\text{C}\equiv\text{N}$  stretching band from 2089 to 2099  $\text{cm}^{-1}$ . In the HCF structure, the inserted cations could influence the  $\text{C}\equiv\text{N}$  bonding strain by the ionic radius difference between  $\text{K}^+$  and  $\text{Cs}^+$  [48]. Moreover, the XRD patterns (Fig.

6(d)) show a change in the crystal structure and the shift of the peaks, marked as the dotted line, to lower  $2\theta$  values indicating higher d-spacing resulted from a larger ionic radius of  $\text{Cs}^+$ . Analogous XRD results were previously reported by Loos-Neskovic's research group [49]. The authors proposed a chemical composition close to  $\text{Cs}_2\text{Cu}[\text{Fe}(\text{CN})_6]$  and concluded that the XRD patterns were ascribed to the appearance of new phases by adsorption of  $\text{Cs}^+$  [49]. The identical analyses were also accompanied with the bulk species and similar results are presented (see Fig. S7). Although  $\text{Cs}^+$  binding mechanism on metal hexacyanoferrates remains controversial, this indicates that the adsorption of  $\text{Cs}^+$  is mainly performed by the cation exchange process [45].

### 3.5. Adsorption isotherms

Equilibrium adsorption isotherms (Fig. 7(a)) were constructed using different initial concentrations of  $\text{Cs}^+$  to evaluate the removal capacities and the affinity of the prepared adsorbents. Initially, the isotherms for the HPC and bulk  $\text{KCuHCF}$  showed a rapid increase in the uptake of  $\text{Cs}^+$  with increasing  $\text{Cs}^+$  concentration, because an abundance of adsorption sites is readily available. At higher concentrations a slower increase is observed due to the competition for accessible binding sites. However, the PC has negligible  $\text{Cs}^+$  capture capacities over a wide range of concentrations, suggesting that the PC has no active sites for  $\text{Cs}^+$  removal. To determine the thermodynamic parameters in terms of  $\text{Cs}^+$  adsorption, the adsorption isotherms for the HPC and bulk were fitted with the well-known Langmuir and Dual-site Langmuir isotherm model. The equations are defined as,

Langmuir isotherm

$$Q = \frac{Q_m b C_e}{1 + b C_e} \quad (5)$$

Dual-site Langmuir isotherm

$$Q = \frac{Q_{m,A} b_A C_e}{1 + b_A C_e} + \frac{Q_{m,B} b_B C_e}{1 + b_B C_e} \quad (6)$$

where,  $Q$  is the amount of  $\text{Cs}^+$  adsorbed per unit weight of adsorbent (mg/g),  $Q_m$  is the saturation loading (mg/g),  $C_e$  is the equilibrium concentration of the adsorbate (mg/L),  $b$  is the affinity coefficient associated with adsorption energy (L/mg), and subscript A and B represent the different binding sites, respectively. Table 3 shows the fitted parameters  $Q_m$  and  $b$ , and the correlation coefficient for both adsorbents. The high correlation coefficient of Dual-site Langmuir model ( $R^2=0.99$  for both bulk and HPC) suggests the presence of different binding sites in the adsorbents. In particular, the binding site of B ( $Q_{m,B}=50$  mg/g) in the HPC accounts for 25% of the total adsorption capacity (200 mg/g), indicating the presence of carboxylate related ion exchange sites as demonstrated by the FTIR and ICP-OES analyses.

Comparing the adsorption uptake, although the HPC shows a lower saturation capacity for  $\text{Cs}^+$  than the bulk adsorbent, these results are unsurprising considering only 17.46 wt% of KCuHCF in the matrix. Assuming  $\text{K}^+$  in the carboxylate adsorption sites is completely exchanged with  $\text{Cs}^+$  at the saturation concentration, where the amounts are determined by the difference of  $\text{K}^+$  measured by ICP-OES and that present in the KCuHCF, the maximum capacity is 667 mg/g KCuHCF for the HPC. This value is 1.6 times higher than the capacity of 410 mg/g obtained for the bulk KCuHCF and corresponds to TEC. The anchored nanoparticles in the oxygen rich

matrix effectively enhance their dispersion as shown by the TEM images and increase the concentration of exchangeable  $K^+$ . As summarized in Table 4, the HPC exhibits notably higher  $Cs^+$  capacity (667 mg/g KCuHCF) compared with previously reported data not only for metal HCF immobilized adsorbents (400 mg/g FC3 in SBA-15 [22] and 621 mg/g HexaCNFe-Cu in chitin bead [3]), but other types of inorganic ion exchangers (280 mg/g KTS-3 [12] and 226 mg/g KMS-1 [13]). This comparison validates the effectiveness of our two-step synthesis procedure to maximize the efficiency of the KCuHCF nanoparticles in the HPC.

### 3.6. Adsorption kinetics

Adsorption kinetics was studied to determine the removal rate and efficiency of a low concentration of  $Cs^+$ . Using DI water, for the bulk KCuHCF as shown in Fig. S8(a), the required time for 90 % removal of  $Cs^+$  is 44 min with no further uptake measured beyond 2 h. However for the HPC (Fig. 7(b)), the uptake process is exceptionally fast with 90 % of  $Cs^+$  ions adsorbed within 9min, and greater than 99.5 %  $Cs^+$  is removed in 30 min. The overall  $Cs^+$  removal at 24 h is 99.9 % (the remaining  $Cs^+$  concentration equal to 1.68 ppb), thus highlighting that even a trace amount of  $Cs^+$  can be extracted using the HPC. The removal kinetics data are fitted with pseudo-second order model to quantify the initial  $Cs^+$  uptake (See Fig. S9 and Table S1).

In order to simulate more realistic conditions, the  $Cs^+$  removal kinetics was also evaluated in seawater. From a practical perspective, the main difficulty for  $Cs^+$  adsorption relates to the extremely low concentrations, below 0.1 %, when in the presence of competing cations such as  $Na^+$ ,  $K^+$ ,  $Ca^{2+}$  and  $Mg^{2+}$ . The concentrations of

$\text{Na}^+$ ,  $\text{K}^+$ ,  $\text{Ca}^{2+}$  and  $\text{Mg}^{2+}$  in seawater (pH = 8) were measured to be 9700, 390, 147, and 1192 ppm, respectively. Note that the competing cations are in extreme excess compared to  $\text{Cs}^+$  ion. In the conditions of 10 ppm  $\text{Cs}^+$  containing seawater, the HPC (Fig. 7(b)) continues to demonstrate significantly faster removal rate than the bulk KCuHCF (Fig. S8(b)). The time required for 90% removal of  $\text{Cs}^+$  is 57 and 104 min for the HPC and the bulk KCuHCF, respectively. Although both adsorbents indicate slower adsorption rate in seawater compared with the case of DI water, due to the high ionic strength [45, 50], they still show very high removal efficiencies greater than 99.5% (Table 5). Moreover, as shown in the inset of Fig. 7(b), the HPC clearly demonstrates faster adsorption and higher removal efficiency as the concentration of  $\text{Cs}^+$  decreases in seawater. The enhanced kinetics of the HPC is attributed to the good dispersion of KCuHCF nanoparticles in the film structure and high ion accessibility to active sites with the aid of 3D-interconnected structure by the hydrogel swelling.

Fig. 7(c) shows the swelling kinetics of the HPC in DI water and seawater. The film was completely hydrated within 5 min and the equilibrium swelling ratios were approximately 8.3 and 3.2 for DI water and seawater, respectively, which implies very fast diffusion of ions to the well dispersed KCuHCF in the film. The fast sorption and high retention of water are closely linked to the meso and macroporous network structure and hydrophilic properties of oxygen functional groups in the HPC.

To evaluate the  $\text{Cs}^+$  selectivity, the distribution coefficient ( $K_d$ ) for seawater kinetics were calculated (Table 5). The bulk KCuHCF shows higher  $K_d$  than HPC in comparable conditions of approximately 10 ppm. But, considering the amount of

KCuHCF in the film and the high removal efficiency of 99.5 %, ion exchange sites in the HPC are very effective for selective removal of  $\text{Cs}^+$ . As compared in Table 5, these  $K_d$  values for the HPC far exceed those reported for metal sulfide KTS-3 [12] and vanadosilicate K-SGU-45 [2]. Moreover, they are notably higher compared with those for metal HCF based adsorbents such as mesoporous silica supported Co or CuHCF [5, 16], and PB/ $\text{Fe}_3\text{O}_4$ /GO [45], indicating a higher affinity of the HPC for  $\text{Cs}^+$ . Especially  $K_d$  and percentage  $\text{Cs}^+$  removal for the HPC increase as the  $\text{Cs}^+$  concentration decreases in the seawater condition having more severe competition between  $\text{Cs}^+$  and other cations, as reported in the case of vanadosilicate K-SGU-45 [2], and prussian blue immobilized resin [24]. These results suggest HPC to be the most effective adsorbent for fast and selective removal of diluted  $\text{Cs}^+$  from large volumes of radioactive contaminated water, thus contributing to significant waste volume reduction and alleviating any long-term environmental impact.

The effect of solution pH on the removal performance of  $\text{Cs}^+$  was investigated from acidic pH = 2 (HCl) to basic pH = 12 (NaOH) conditions, in the presence of 11 ppm  $\text{Cs}^+$  solution. The HPC exhibits superior removal efficiency (97.8 – 99.9 %) over the entire pH range, as shown in Fig. 7(d). At pH 12, the removal performance (97.8 %) slightly deteriorated, which may be attributed to the decomposition of HCF in a high alkaline condition as reported in previous studies [1, 24, 45, 51]. This decomposition is supported by the detected amounts of Cu in solution using ICP-MS. For the sample immersed in pH 12 solution, Cu concentration was 1.8 ppm which is approximately 420 times higher than the average value of 4.3 ppb for all other samples, indicating that a small amount of KCuHCF decomposes during extended

contact (24 h) with the highly alkaline solution. Below pH 10, the Cs<sup>+</sup> capture performance of the HPC is outstanding with a removal efficiency of 99.9%. Even in the presence of abundant H<sup>+</sup> (pH = 2), the percentage of Cs<sup>+</sup> removal remains very high, reflecting the excellent Cs<sup>+</sup> selective properties of the HPC. These results demonstrate that the HPC can be effective and stable for the separation of Cs<sup>+</sup> over a broad range of pHs.

#### 4. Conclusions

KCuHCF embedded hydrogel film adsorbent (HPC) has been prepared by a facile two-step method of simultaneous Cu dispersion and incorporation, and K<sub>4</sub>[Fe(CN)<sub>6</sub>] diffusion assisted by acetone evaporation. The synthesized hydrogel film exhibits highly dispersed KCuHCF nanoparticles in the 3D-interconnected porous hydrogel structure. The ion exchange mechanism for KCuHCF is supported by the comparable analyses for the pristine and Cs<sup>+</sup> exchanged adsorbents. The as-obtained HPC demonstrates superior Cs<sup>+</sup> adsorption capacities and significantly faster kinetics compared with those of the bulk KCuHCF. This novel HPC adsorbent exhibits very high Cs<sup>+</sup> capturing performance of 667 mg/g KCuHCF at the saturated concentration. Furthermore, the sample can provide near complete Cs<sup>+</sup> removal (99.9 %) with enhanced removal kinetics (above 99.5% within 30 min) in DI water and almost unaltered Cs<sup>+</sup> removal efficiency above 99.5 %, even when tested in seawater. In particular, the HPC demonstrates an unprecedented increase of K<sub>d</sub> up to  $7.7 \times 10^5$  mL/g with decreasing Cs<sup>+</sup> concentration, indicating the exceptional Cs<sup>+</sup> affinity over all other competing cations. These enhanced adsorption properties are closely

associated with the combined effects including rich  $K^+$  contents in KCuHCF, high dispersion of the nanoparticles in the matrix, and the fast swelling kinetics of the hydrogel matrix. In addition, it represents a system that is stable and provides excellent removal efficiency of  $Cs^+$  over a broad pH range. Therefore, combined with the simple sample preparation and low production cost, this synthesized HPC is one of the most promising adsorbents for the rapid and selective removal of  $Cs^+$  from contaminated environments.

### Acknowledgements

This work was supported by the UK-Korea Joint Research Program through NRF grants (NRF-2015M2A7A1000219) funded by the Ministry of Science, ICT, and Future Planning. D. Harbottle acknowledges the support from the Engineering and Physical Sciences Research Council grant number EP/M02646/1.

### References

- [1] H. Yang, H. Li, J. Zhai, L. Sun, Y. Zhao, H. Yu, Magnetic prussian blue/graphene oxide nanocomposites caged in calcium alginate microbeads for elimination of cesium ions from water and soil, *Chemical Engineering Journal* 246 (2014) 10-19.
- [2] S.J. Datta, W.K. Moon, D.Y. Choi, I.C. Hwang, K.B. Yoon, A Novel Vanadosilicate with Hexadeca-Coordinated  $Cs^+$  Ions as a Highly Effective  $Cs^+$  Remover, *Angew Chem Int Edit* 53 (2014) 7203-7208.
- [3] T. Vincent, C. Vincent, Y. Barre, Y. Guari, G. Le Saout, E. Guibal, Immobilization of metal hexacyanoferrates in chitin beads for cesium sorption: synthesis and characterization, *Journal of Materials Chemistry A* 2 (2014) 10007-10021.
- [4] R. Chen, H. Tanaka, T. Kawamoto, M. Asai, C. Fukushima, M. Kurihara, M. Ishizaki, M. Watanabe, M. Arisaka, T. Nankawa, Thermodynamics and mechanism studies on electrochemical removal of cesium ions from aqueous solution using a nanoparticle film of copper hexacyanoferrate, *ACS Appl Mater Interfaces* 5 (2013) 12984-12990.
- [5] C. Delchet, A. Tokarev, X. Dumail, G. Toquer, Y. Barré, Y. Guari, C. Guerin, J. Larionova, A. Grandjean,

Extraction of radioactive cesium using innovative functionalized porous materials, *RSC Advances* 2 (2012) 5707.

[6] A. Nilchi, R. Saberi, M. Moradi, H. Azizpour, R. Zarghami, Adsorption of cesium on copper hexacyanoferrate–PAN composite ion exchanger from aqueous solution, *Chemical Engineering Journal* 172 (2011) 572-580.

[7] P.K. Sinha, P.K. Panicker, R.V. Amalraj, V. Krishnasamy, Treatment of radioactive liquid waste containing caesium by indigenously available synthetic zeolites: A comparative study, *Waste Management* 15 (1995) 149-157.

[8] H.-L. Chang, W.-H. Shih, A General Method for the Conversion of Fly Ash into Zeolites as Ion Exchangers for Cesium, *Industrial & Engineering Chemistry Research* 37 (1998) 71-78.

[9] H.M. Liu, A. Yonezawa, K. Kumagai, M. Sano, T. Miyake, Cs and Sr removal over highly effective adsorbents ETS-1 and ETS-2, *Journal of Materials Chemistry A* 3 (2015) 1562-1568.

[10] B.R. Cherry, M. Nyman, T.M. Alam, Investigation of cation environment and framework changes in silicotitanate exchange materials using solid-state  $^{23}\text{Na}$ ,  $^{29}\text{Si}$ , and  $^{133}\text{Cs}$  MAS NMR, *Journal of Solid State Chemistry* 177 (2004) 2079-2093.

[11] J.L. Mertz, Z.H. Fard, C.D. Malliakas, M.J. Manos, M.G. Kanatzidis, Selective Removal of  $\text{Cs}^+$ ,  $\text{Sr}^{2+}$ , and  $\text{Ni}^{2+}$  by  $\text{K}_2\text{xMgxSn}_3\text{-xS}_6$  ( $\text{x}=0.5\text{-}1$ ) (KMS-2) Relevant to Nuclear Waste Remediation, *Chemistry of Materials* 25 (2013) 2116-2127.

[12] D. Sarma, C.D. Malliakas, K.S. Subrahmanyam, S.M. Islama, M.G. Kanatzidis,  $\text{K}_2\text{xSn}_4\text{-xS}_8\text{-x}$  ( $\text{x}=0.65\text{-}1$ ): a new metal sulfide for rapid and selective removal of  $\text{Cs}^+$ ,  $\text{Sr}^{2+}$  and  $\text{UO}_2^{2+}$  ions, *Chem Sci* 7 (2016) 1121-1132.

[13] M.J. Manos, M.G. Kanatzidis, Highly Efficient and Rapid  $\text{Cs}^+$  Uptake by the Layered Metal Sulfide  $\text{K}_2\text{xMnxSn}_3\text{-xS}_6$  (KMS-1), *Journal of the American Chemical Society* 131 (2009) 6599-6607.

[14] S.B. Yang, N. Okada, M. Nagatsu, The highly effective removal of  $\text{Cs}^+$  by low turbidity chitosan-grafted magnetic bentonite, *Journal of Hazardous Materials* 301 (2016) 8-16.

[15] S.B. Yang, C. Han, X.K. Wang, M. Nagatsu, Characteristics of cesium ion sorption from aqueous solution on bentonite- and carbon nanotube-based composites, *Journal of Hazardous Materials* 274 (2014) 46-52.

[16] R. Turgis, G. Arrachart, C. Delchet, C. Rey, Y. Barre, S. Pellet-Rostaing, Y. Guari, J. Larionova, A. Grandjean, An Original "Click and Bind" Approach for Immobilizing Copper Hexacyanoferrate Nanoparticles on Mesoporous Silica, *Chemistry of Materials* 25 (2013) 4447-4453.

[17] R. Yi, G. Ye, F. Wu, M. Wen, X. Feng, J. Chen, Highly efficient removal of  $^{137}\text{Cs}$  in seawater by potassium titanium ferrocyanide functionalized magnetic microspheres with multilayer core-shell structure, *RSC Advances* 4 (2014) 37600-37608.

[18] H.X. Zhang, X. Zhao, J.Y. Wei, F.Z. Li, Removal of cesium from low-level radioactive wastewaters using magnetic potassium titanium hexacyanoferrate, *Chemical Engineering Journal* 275 (2015) 262-270.

[19] C.D. Wessells, R.A. Huggins, Y. Cui, Copper hexacyanoferrate battery electrodes with long cycle life and high power, *Nature Communications* 2 (2011).

[20] J. Causse, A. Tokarev, J. Ravaux, M. Moloney, Y. Barre, A. Grandjean, Facile one-pot synthesis of copper hexacyanoferrate nanoparticle functionalised silica monoliths for the selective entrapment of  $\text{Cs-}^{137}$ , *Journal of Materials Chemistry A* 2 (2014) 9461-9464.

[21] M.A. Olatunji, M.U. Khandaker, H.N.M.E. Mahmud, Y.M. Amin, Influence of adsorption parameters on cesium uptake from aqueous solutions- a brief review, *RSC Advances* 5 (2015) 71658-71683.

- [22] J. Qian, J.Q. Ma, W.W. He, D.B. Hua, Facile Synthesis of Prussian Blue Derivate-Modified Mesoporous Material via Photoinitiated Thiol-Ene Click Reaction for Cesium Adsorption, *Chem-Asian J* 10 (2015) 1738-1744.
- [23] C. Dwivedi, S.K. Pathak, M. Kumar, S.C. Tripathi, P.N. Bajaj, Preparation and characterization of potassium nickel hexacyanoferrate-loaded hydrogel beads for the removal of cesium ions, *Environ Sci-Wat Res* 1 (2015) 153-160.
- [24] H.J. Yang, H.Y. Li, J.L. Zhai, H.W. Yu, In situ growth of Prussian blue nanocrystal within Fe<sup>3+</sup> crosslinking PAA resin for radiocesium highly efficient and rapid separation from water, *Chemical Engineering Journal* 277 (2015) 40-47.
- [25] X. Sun, T. Fujimoto, H. Uyama, Fabrication of a poly(vinyl alcohol) monolith via thermally impacted non-solvent-induced phase separation, *Polym J* 45 (2013) 1101-1106.
- [26] Y. Yang, H. Gao, L. Zheng, Anhydrous proton exchange membranes at elevated temperatures: effect of protic ionic liquids and crosslinker on proton conductivity, *RSC Advances* 5 (2015) 17683-17689.
- [27] Z. Chen, M. Deng, Y. Chen, G. He, M. Wu, J. Wang, Preparation and performance of cellulose acetate/polyethyleneimine blend microfiltration membranes and their applications, *Journal of Membrane Science* 235 (2004) 73-86.
- [28] D. Mawad, E. Stewart, D.L. Officer, T. Romeo, P. Wagner, K. Wagner, G.G. Wallace, A Single Component Conducting Polymer Hydrogel as a Scaffold for Tissue Engineering, *Advanced Functional Materials* 22 (2012) 2692-2699.
- [29] Z. Li, Y. Su, B. Xie, X. Liu, X. Gao, D. Wang, A novel biocompatible double network hydrogel consisting of konjac glucomannan with high mechanical strength and ability to be freely shaped, *Journal of Materials Chemistry B* 3 (2015) 1769-1778.
- [30] B. Jiang, W.L. Hom, X. Chen, P. Yu, L.C. Pavelka, K. Kisslinger, J.B. Parise, S.R. Bhatia, R.B. Grubbs, Magnetic Hydrogels from Alkyne/Cobalt Carbonyl-Functionalized ABA Triblock Copolymers, *Journal of the American Chemical Society* 138 (2016) 4616-4625.
- [31] A. Tokarev, P. Agulhon, J. Long, F. Quignard, M. Robitzer, R.A.S. Ferreira, L.D. Carlos, J. Larionova, C. Guerin, Y. Guari, Synthesis and study of Prussian blue type nanoparticles in an alginate matrix, *Journal of Materials Chemistry* 22 (2012) 20232-20242.
- [32] Y. Guari, J. Larionova, K. Molvinger, B. Folch, C. Guerin, Magnetic water-soluble cyano-bridged metal coordination nano-polymers, *Chemical Communications* (2006) 2613-2615.
- [33] J. Sun, L.N. Yu, J. Bi, C.S. Zhang, S.F. Liu, F. Zhu, Q.L. Yang, Peanut protein-polyvinyl alcohol composite fibers extruded from an ionic liquid, *Rsc Advances* 3 (2013) 10619-10622.
- [34] B.C.E. Makhubela, A. Jardine, G.S. Smith, Rh(I) complexes supported on a biopolymer as recyclable and selective hydroformylation catalysts, *Green Chem* 14 (2012) 338-347.
- [35] A. Takahashi, N. Minami, H. Tanaka, K. Sue, K. Minami, D. Parajuli, K.M. Lee, S.I. Ohkoshi, M. Kurihara, T. Kawamoto, Efficient synthesis of size-controlled open-framework nanoparticles fabricated with a micro-mixer: route to the improvement of Cs adsorption performance, *Green Chem* 17 (2015) 4228-4233.
- [36] S. Liu, G.L. Pan, G.R. Li, X.P. Gao, Copper hexacyanoferrate nanoparticles as cathode material for aqueous Al-ion batteries, *Journal of Materials Chemistry A* 3 (2015) 959-962.
- [37] C. Dwivedi, A. Kumar, K.K. Singh, A.K. Juby, M. Kumar, P.K. Wattal, P.N. Bajaj, Copper hexacyanoferrate-polymer composite beads for cesium ion removal: Synthesis, characterization, sorption, and kinetic studies, *J Appl Polym Sci* 129 (2013) 152-160.

- [38] L.V. Thomas, U. Arun, S. Remya, P.D. Nair, A biodegradable and biocompatible PVA-citric acid polyester with potential applications as matrix for vascular tissue engineering, *J Mater Sci-Mater M* 20 (2009) 259-269.
- [39] A. Singhal, M. Kaur, K.A. Dubey, Y.K. Bhardwaj, D. Jain, C.G.S. Pillai, A.K. Tyagi, Polyvinyl alcohol-In<sub>2</sub>O<sub>3</sub> nanocomposite films: synthesis, characterization and gas sensing properties, *RSC Advances* 2 (2012) 7180-7189.
- [40] A. Pourjavadi, B. Pournadiei, M. Doroudian, S. Azari, Preparation of PVA nanocomposites using salep-reduced graphene oxide with enhanced mechanical and biological properties, *RSC Advances* 5 (2015) 92428-92437.
- [41] C. Cheng, Y. Wen, X. Xu, H. Gu, Tunable synthesis of carboxyl-functionalized magnetite nanocrystal clusters with uniform size, *Journal of Materials Chemistry* 19 (2009) 8782-8788.
- [42] Q. Zhao, J. Qian, M. Zhu, Q. An, Facile fabrication of polyelectrolyte complex/carbon nanotube nanocomposites with improved mechanical properties and ultra-high separation performance, *Journal of Materials Chemistry* 19 (2009) 8732-8740.
- [43] C. Ling, F. Liu, Z. Pei, X. Zhang, M. Wei, Y. Zhang, L. Zheng, J. Zhang, A. Li, B. Xing, Citric Acid Enhanced Copper Removal by a Novel Multi-amines Decorated Resin, *Sci Rep-Uk* 5 (2015) 9944.
- [44] T. Suemoto, R. Fukaya, A. Asahara, M. Nakajima, H. Tokoro, S. Ohkoshi, Dynamics of photoinduced phase transitions in hexacyanoferrate studied by infrared and Raman spectroscopy, *physica status solidi (b)* 248 (2011) 477-481.
- [45] H.J. Yang, L. Sun, J.L. Zhai, H.Y. Li, Y. Zhao, H.W. Yu, In situ controllable synthesis of magnetic Prussian blue/graphene oxide nanocomposites for removal of radioactive cesium in water, *Journal of Materials Chemistry A* 2 (2014) 326-332.
- [46] X. Wang, Q. Xiang, B. Liu, L. Wang, T. Luo, D. Chen, G. Shen, TiO<sub>2</sub> modified FeS Nanostructures with Enhanced Electrochemical Performance for Lithium-Ion Batteries, *Sci Rep-Uk* 3 (2013) 2007.
- [47] T. Vincent, C. Vincent, E. Guibal, Immobilization of Metal Hexacyanoferrate Ion-Exchangers for the Synthesis of Metal Ion Sorbents-A Mini-Review, *Molecules* 20 (2015) 20582-20613.
- [48] H.-W. Lee, R.Y. Wang, M. Pasta, S. Woo Lee, N. Liu, Y. Cui, Manganese hexacyanomanganate open framework as a high-capacity positive electrode material for sodium-ion batteries, *Nat Commun* 5 (2014).
- [49] C. Loos-Neskovic, S. Ayrault, V. Badillo, B. Jimenez, E. Garnier, M. Fedoroff, D.J. Jones, B. Merinov, Structure of copper-potassium hexacyanoferrate (II) and sorption mechanisms of cesium, *Journal of Solid State Chemistry* 177 (2004) 1817-1828.
- [50] H.B. Bradl, Adsorption of heavy metal ions on soils and soils constituents, *Journal of Colloid and Interface Science* 277 (2004) 1-18.
- [51] R.Z. Chen, H. Tanaka, T. Kawamoto, M. Asai, C. Fukushima, H.T. Na, M. Kurihara, M. Watanabe, M. Arisaka, T. Nankawa, Selective removal of cesium ions from wastewater using copper hexacyanoferrate nanofilms in an electrochemical system, *Electrochim Acta* 87 (2013) 119-125.

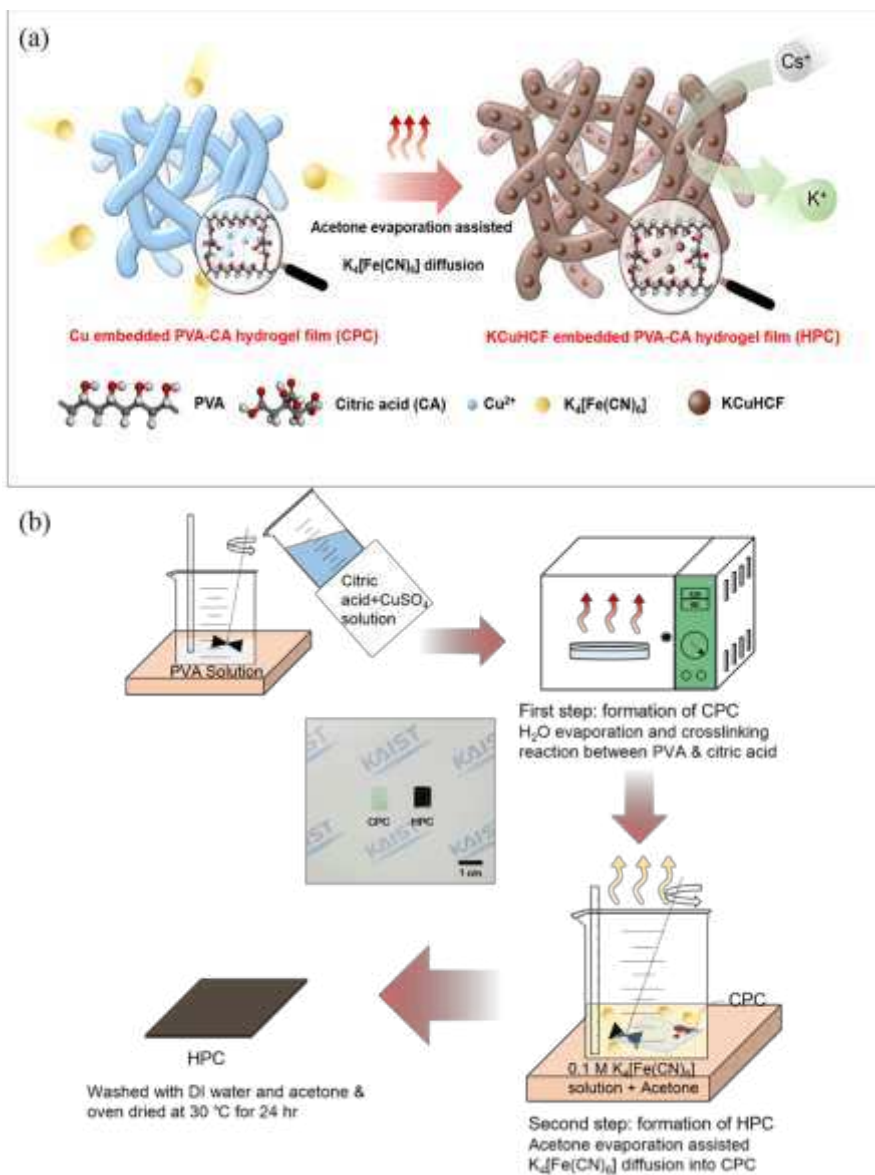


**Fig. 1** (a) Schematic representation of CPC and HPC. (b) Two-step synthesis procedure for HPC.

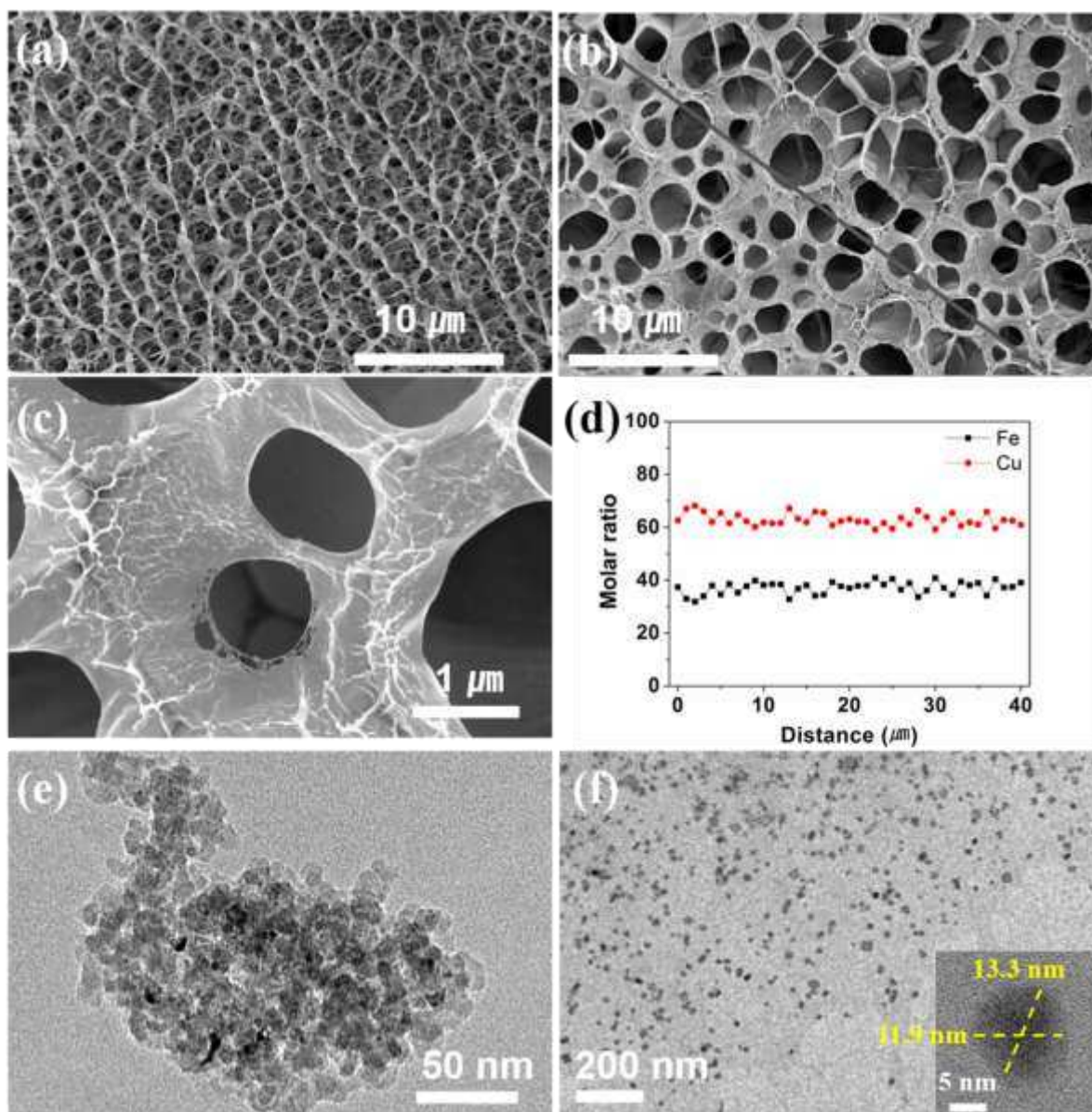


**Fig. 2.** SEM images of (a) PC and (b), (c) HPC. (d) Fe and Cu atomic ratios in HPC by EDS measurements. TEM images of (e) bulk KCuHCF and (f) HPC (Inset: high-resolution TEM image of KCuHCF in HPC).

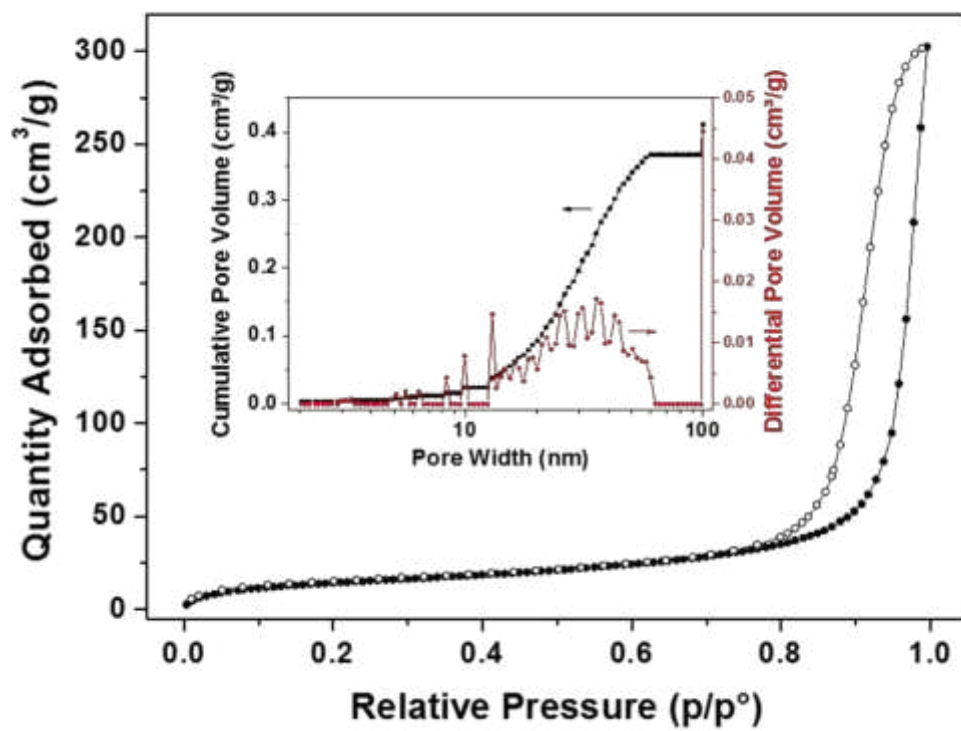


**Fig. 3.** N<sub>2</sub> adsorption isotherm at 77 K for HPC (Inset: NLDFT pore size distributions).

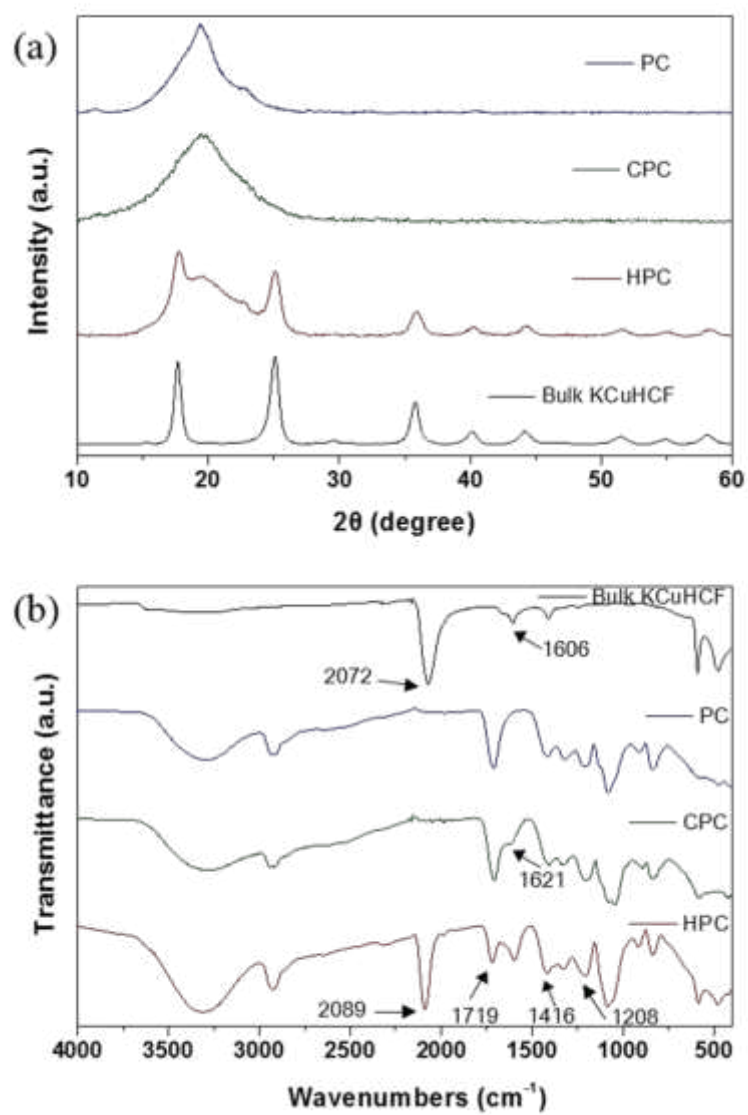


**Fig. 4.** (a) XRD patterns and (b) IR spectra for bulk KCuHCF, PC, CPC, and HPC.

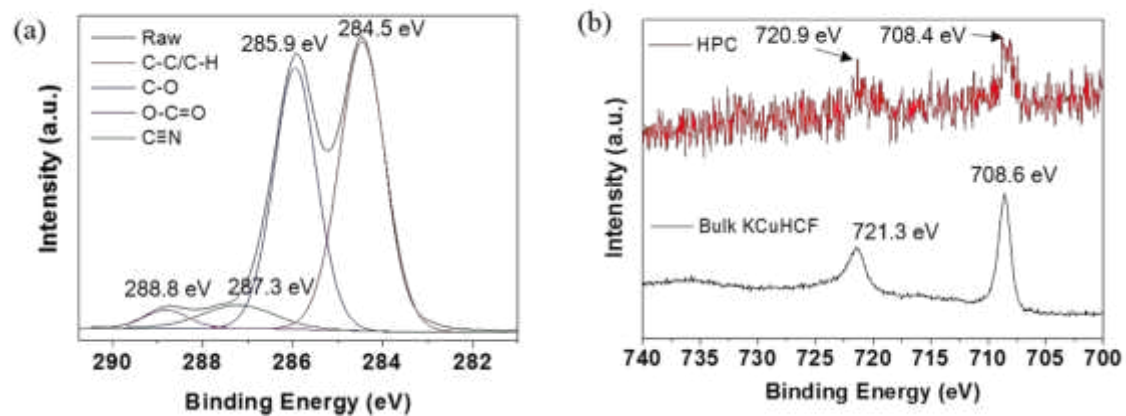


**Fig. 5.** XPS (a) C1s spectra of HPC and (b) Fe2p spectra of HPC and bulk KCuHCF.

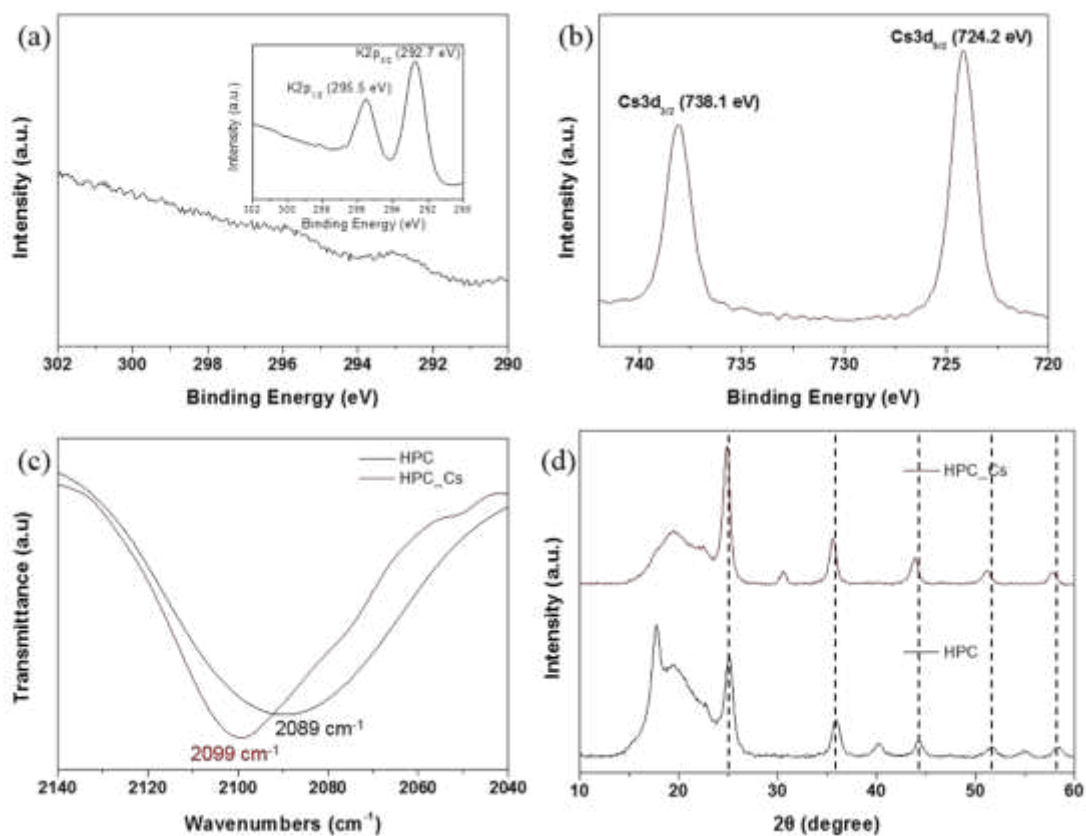


**Fig. 6.** (a) K2p XPS spectra of HPC after  $\text{Cs}^+$  adsorption (Inset: K2p spectra before  $\text{Cs}^+$  adsorption) and (b) Cs3d XPS spectra of HPC after  $\text{Cs}^+$  adsorption. (c) IR spectra and (d) XRD patterns of HPC before and after  $\text{Cs}^+$  adsorption.

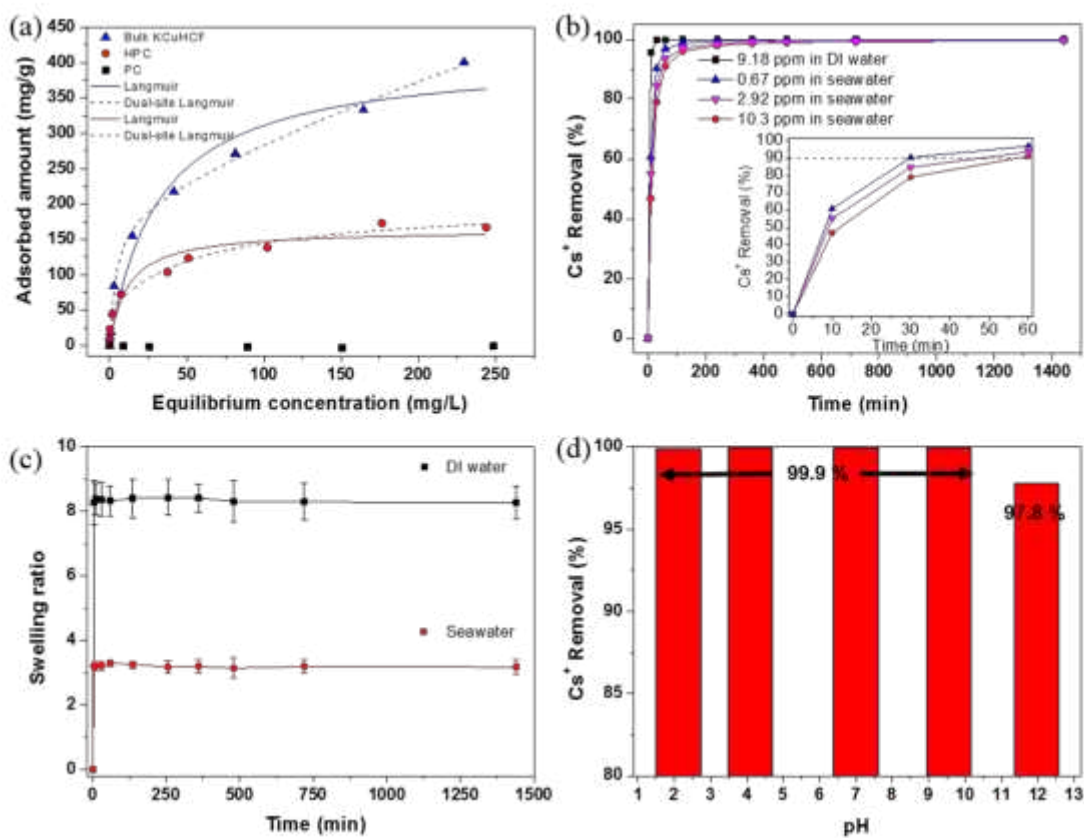


**Fig. 7.** (a) Cs<sup>+</sup> adsorption isotherms for PC, HPC, and bulk KCuHCF with Langmuir and Dual-site Langmuir fitting curves. (b) Cs<sup>+</sup> removal kinetics of HPC (Inset: enlarged view of Cs<sup>+</sup> removal kinetics in seawater up to removal time of 60 min). (c) swelling kinetics of HPC in DI water and seawater. (d) Cs<sup>+</sup> removal efficiency of HPC in various pH conditions ( $C_0 \approx 11$

**Table 1** Reaction conditions in diffusion step and chemical compositions of the as-prepared CPC and HPC.

Sample	Reaction conditions		Chemical compositions (wt%)	
	Acetone-treatment	Heat-treatment	Cu	Fe
Pristine CPC	-	-	5.23	-
W-RT <sup>a</sup>	-	-	2.15	1.37
W-35	-	35°C for 2hr	2.77	1.77
WA-RT <sup>a</sup>	200 ml of acetone	-	4.02	1.16
WA-35	200 ml of acetone	35°C for 2hr	4.18	3.41

<sup>a</sup> Room temperature

**Table 2** ICP-OES elemental analyses of HPC and bulk KCuHCF.

Sample	Elemental analysis		
	Chemical compositions <sup>a</sup>	TEC <sup>b</sup>	IEC <sup>c</sup>
HPC	$K_{1.72}Cu[Fe(CN)_6]_{0.93}$	695	17.46
Bulk KCuHCF	$K_{0.72}Cu[Fe(CN)_6]_{0.68}$	405	100

<sup>a</sup>  $K_{4x-2}Cu[Fe(CN)_6]_x$ , where x indicates  $[Fe(CN)_6]/Cu$ . <sup>b</sup> TEC, Theoretical exchange capacity (mg  $Cs^+$ /g KCuHCF). <sup>c</sup> IEC, Ion-exchanger (KCuHCF) content in the composite (% , w/w).

**Table 3** Langmuir and Dual-site Langmuir isotherm constants of HPC and bulk KCuHCF.

Sample	Langmuir isotherm constants				Dual-site Langmuir isotherm constants				
	$Q_m$ (mg/g)	$Q_m^*$ (mg/g) <sup>a</sup>	$b$ (L/mg)	$R^2$	$Q_{mA}$ (mg/g)	$b_A$ (L/mg)	$Q_{mB}$ (mg/g)	$b_B$ (L/mg)	$R^2$
HPC	164	667	0.08	0.94	150	0.02	50	5.37	0.99
Bulk KCuHCF	410	410	0.03	0.97	1167	$9.68 \times 10^{-4}$	187	0.24	0.99

<sup>a</sup>  $Q_m^*$ : mg Cs<sup>+</sup>/g KCuHCF.

**Table 4** Comparison of Cs<sup>+</sup> capacities in mg per gram of ion exchanger for different adsorbents.

Adsorbents	Capacity (mg/g ion exchanger)	Reference
SBA-15@FC1	372	[22]
SBA-15@FC2	364	[22]
SBA-15@FC3	400	[22]
COFC@ Silica-Py	173	[5]
COFC@ Glass-Py	173	[5]
SBA-CuFC	286	[16]
GP-CuGC	328	[16]
HexaCNFe-Zn in chitin bead	508	[3]
HexaCNFe-Cu in chitin bead	621	[3]
KTS-3	280	[12]
KMS-1	226	[13]
HPC	667	This work

**Table 5**  $K_d$  values and removal efficiency of  $Cs^+$  for various ion exchangers in the presence of competing cations.

Adsorbent	$C_0$ (ppm)	$K_d$ (mL/g)	% Removal	Reference
Bulk KCuHCF	10.16 ppm in seawater	$5.46 \times 10^6$	99.87	This work
HPC	10.30 ppm in seawater	$2.33 \times 10^5$	99.57	This work
HPC	2.92 ppm in seawater	$2.95 \times 10^5$	99.66	This work
HPC	0.67 ppm in seawater	$7.74 \times 10^5$	99.87	This work
KTS-3	7.4 ppm in 0.1 M $Na^+$	$4.4 \times 10^3$	N/A	[12]
K-SGU-45	1 ppm in seawater	$1.8 \times 10^4$	N/A	[2]
CoFC @Silica-Py	10 ppm in seawater	$>10^4$	N/A	[5]
SBA-CuFC	13 ppm in seawater	$5.8 \times 10^3$	N/A	[16]
5.1@SiO <sub>2</sub>	0.01 ppb in seawater	$1.1 \times 10^5$	N/A	[20]
PB/Fe <sub>3</sub> O <sub>4</sub> /GO	10 ppm in seawater	$5.1 \times 10^4$	N/A	[45]